Numerical simulation of compressible flow with shocks using the OUCS2 upwind compact scheme

AbhishekKundu

Department of Mechanical Engineering, Swami Vivekananda Institute of Science & Technology, West Bengal, India.
Corresponding author: abhishekkundu45@gmail.com

Abstract

The OUCS2 upwind compact scheme for calculation of first derivatives in the Euler and Navier-Stokes equations is the focus of the present paper. Derived and analyzed by Sengupta et al. and primarily meant for incompressible flow problems, the scheme has recently been applied to compressible flow with shocks. To handle shocks effectively, a combination of second and fourth derivative artificial dissipation terms were used by Sengupta et al., instead of the inbuilt sixth derivative dissipation of the OUCS2. For unsteady flow problems with shocks and vortices, use of high order numerical dissipation is desirable for proper resolution of small scale structures. In a present paper we show that when used with flux limiters, one can use the inbuilt high order dissipation in smooth regions and still bring down the scheme to small stencil formulae with low order dissipation near shocks. The basic solver is built upon the AUSM$^+$ algorithm. OUCS2 comes in while computing the left and right states of the primitive variables at the cell faces, requiring little effort to modify an existing AUSM$^+$ based solver to a high resolution version with the help of OUCS2. We demonstrate the procedure for a number of problems in one and two dimensions solving the Euler equations.

Key words: AUSM$^+$, Compressible flow, Euler equations, Flux limiter, High Mach number

Introduction

Numerical simulation of Euler or Navier-Stokes equations using finite difference or finite volume based methods requires discretization of the first and second derivative terms in terms of values of the variables at discrete grid locations. Such formulae may be explicit - linking the derivative at a grid location to the variable value in a chosen neighbourhood - or they may be in the form of an implicit relation which includes neighbourhood derivatives in a single formula. The latter class of schemes are known as compact schemes. Utilizing compact schemes for fluid dynamics applications can be linked to Anderi I. Tolstykh, who suggested their use back in 1972 (Tolstykh, 1994a). The various compact schemes derived by Tolstykh and his group belong to the CUD (Compact Upwind Differencing) family of schemes. Developments on the third and fifth order CUD schemes may be found in (Tolstykh, 1994a,b). Their application to compressible flow problems are mentioned in (Tolstykh, 1994a, 1973; Ravichandran, 1994, 1997; Tolstykh and Lipavskii, 1998). Application of compact schemes to compressible solvers demands special care due to the presence of sharp gradients in the form of shock waves. One needs to apply low order numerical dissipation locally at a shock for stable computation. For compressible applications, the Euler or Navier-Stokes equations are usually discretized in a conservative form involving fluxes at the cell faces. One may, therefore, derive the compact scheme in a form suitable for the flux calculation. This approach has been followed in (Tolstykh, 1994a; Pirozzoli, 2002). Alterna-

tively, the compact derivative scheme may be applied straightaway in a nonconservative manner, as demonstrated in (Sengupta et al., 2013). Though the governing equations are in conservative form, in the latter approach, dependence on a pressure based switch leads to non-cancellation of variable values in the interior, and boundary stencils contribute to the same effect near the boundaries.

It is the demand for schemes with high spectral accuracy in smooth regions and highly dissipative schemes at the shock that has led to the development of a number of methods addressing this issue. Rizzetta and Morgan, (2008) recommends use of central compact schemes which are nondissipative, together with compact filtering schemes. The basic solver is based on an implicit approximately factored finite difference scheme, and in the words of the authors - 'nonlinear artificial dissipation terms are also appended to the implicit operators to augment stability.' This does not allow estimation of the capacity of the filtering technique Rizzetta and Morgan (2008) alone in the presence of strong shocks. An explicit solver would be ideal for the evaluation of the compact derivative and filtering schemes. This is followed by Meinke et al. (Meinke et al., 2002), who employ an explicit AUSM based solver together with compact derivative and filtering schemes. This, however, has been tested only for large eddy simulation of planar turbulent jets. Kawai et al. (Kawai et al., 2010) use a combination of compact derivative scheme and a filtering scheme as above, together with a localized artificial diffusivity (LAD) which activates near shocks. This method has primarily been tested for large eddy simulation of compressible turbulent flows. Currently the more popular methods for application of compact schemes to compressible shock dominated flows involve the ENO or WENO schemes. Here compact derivatives enter as part of a hybridization strategy (Pirozzoli, 2002). In these methods, the compact scheme operates in the smoother regions, leaving the task of shock capturing to the ENO/WENO scheme. The general idea in a WENO scheme is to compute the numerical flux from a combination of a number of candidate stencils (Jiang and Shu, 1996), which renders implementation of the method complex. Complexity is only enhanced in a hybridized form with a compact scheme.

The OUCS2 was derived and analyzed in the wavenumber space in (Sengupta et al., 2003). Being a fifth-order upwind compact scheme, it possesses high accuracy in the wavenumber space and low numerical dissipation at lower wavenumbers. As mentioned before, when applied with a combination of fourth and second derivative numerical dissipation, the scheme partly loses this attractive property of low dissipation in the lower wavenum-

ber range. In order to retain its inbuilt sixth derivative driven numerical dissipation, we felt encouraged to apply it in combination with a flux limiter, particularly after noticing the success achieved by application of limiters with high resolution explicit conservative schemes (Hahn and Drikakis, 2009; Halder et al., 2013; Dora et al., 2014; Kundu and De, 2014). The last three references have dealt with shock and vortex dominated flows simulated by an explicit AUSM$^+$ based solver with explicit high resolution schemes. In the following sections, we show that a similar strategy is also possible for the OUCS2 scheme - written as a cell-face interpolation scheme - and this yields accurate results.
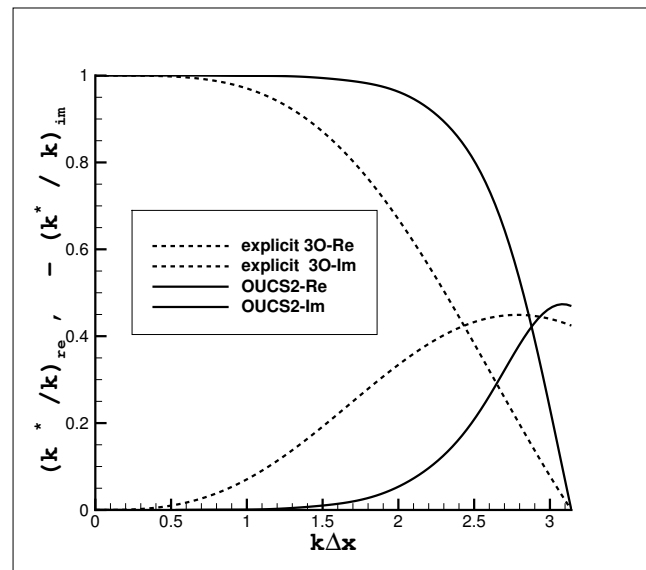
Fig. 1. Real and imaginary components of the modified wavenumber of the OUCS2. For comparison, the modified wavenumber components of a third-order explicit upwind scheme (Eq. 7) is also shown.

Numerical method

The Euler equations for compressible flow may be written concisely as

$$\frac{\partial q}{\partial t} + \frac{\partial f}{\partial x} + \frac{\partial g}{\partial y} = 0. \tag{1}$$

The variables can be expanded as:

$$q = \begin{pmatrix} \rho \\ \rho u \\ \rho v \\ \rho E \end{pmatrix}, f = \begin{pmatrix} \rho u \\ \rho u^2 + p \\ \rho uv \\ (\rho E + p)u \end{pmatrix}, g = \begin{pmatrix} \rho v \\ \rho uv \\ \rho v^2 + p \\ (\rho E + p)v \end{pmatrix}.$$

Energy is given by $\rho E = \frac{p}{\gamma - 1} + \frac{1}{2}\rho\left(u^2 + v^2\right)$. u, v are the velocity components in the x- and y-directions, respectively. ρ denotes the gas density and p denotes the

pressure. To comprehend the application of the compact scheme in the place of MUSCL-type cell-face interpolation formula, let us have a look at how the cell-face flux is written in AUSM$^+$ (Liou, 1996):

$$f_{i+\frac{1}{2},j} = a_{i+\frac{1}{2},j}[0.5m_{i+\frac{1}{2},j}\,(\Phi_L + \Phi_R) - 0.5\Psi_{i+\frac{1}{2},j}$$
$$(\Phi_R - \Phi_L)]. \tag{2}$$

In the above, we have omitted the pressure term that appears if the the above equation is for the x-momentum equation. $\Psi_{i+\frac{1}{2},j} = |m_{i+\frac{1}{2},j}|$ in the original version of the AUSM$^+$. We use a slightly modified formula which retains non-zero numerical dissipation as Mach number goes to zero (De and Murugan, 2011). The quantities Φ_L and Φ_R represent the left and right states composed of the left and right states of the primitive variables, as suggested by Liou (Liou, 1996). The OUCS2 compact scheme has been applied as an interpolation formula to compute these left and right states of the primitive variables, as explained below.

The OUCS2 compact upwind scheme for calculation of a first derivative is written as,

$$b_1 u'_{j-1} + b_2 u'_j + b_3 u'_{j+1} = (a_{-2}u_{j-2} + a_{-1}u_{j-1}$$
$$+ a_0 u_j + a_1 u_{j+1} + a_2 u_{j+2})/h. \tag{3}$$

In Eq. 3, $b_1 = \frac{b_2}{3} - \frac{\alpha}{12}$, $b_3 = \frac{b_2}{3} + \frac{\alpha}{12}$, $a_{\mp 2} = \mp\frac{b_2}{36} + \frac{\alpha}{72}$, $a_{\mp 1} = \mp\frac{7b_2}{9} + \frac{\alpha}{9}$, $a_0 = -\frac{\alpha}{4}$, with $b_2 = 36$. α is an upwinding parameter. The recommended value of α is -40 (Sengupta et al., 2003). The real and imaginary components of the modified wavenumber of the OUCS2 are displayed in Fig. 1. In the form of an interpolation scheme for the cell-faces, the OUCS2 scheme thus becomes:

$$b_1 u_{j-\frac{1}{2}} + b_2 u_{j+\frac{1}{2}} + b_3 u_{j+\frac{3}{2}} = e_{-1}u_{j-1} + e_0 u_j$$
$$+ e_1 u_{j+1} + e_2 u_{j+2}. \tag{4}$$

The new coefficients are $e_{-1} = \frac{b_2}{36} - \frac{\alpha}{72}$, $e_0 = \frac{29b_2}{36} - \frac{\alpha}{8}$, $e_1 = \frac{29b_2}{36} + \frac{\alpha}{8}$ and $e_2 = \frac{b_2}{36} + \frac{\alpha}{72}$.

The following boundary closure is used for non-periodic boundaries:

$$u_{j+\frac{1}{2}} + \frac{6}{10}u_{j+\frac{3}{2}} = \frac{3u_j + 12u_{j+1} + u_{j+2}}{10}, \tag{5}$$

The distortion in the modified wavenumber at the near-boundary points introduced by this one-sided closure does not affect the solution as we use explicit upwind schemes of third and fifth order at these points.

Once the cell-face values of the primitive variables are available from the above equation, a TVD limiter is applied, as is done in any high resolution solver that uses an explicit cell-face interpolation scheme (Kundu and De, 2014). The form of OUCS2 as given in Eq. 4 makes it possible to apply the OUCS2 in a fully conservative form. The CUD-3 upwind scheme described previously had been tested in both conservative and non-conservative forms (Tolstykh, 1994a). The author suggested avoiding the non-conservative form for computing discontinuous solutions; the conservative option was viewed as a 'good choice.' The conservative form of the OUCS2, suggested above, has the same advantage over its non-conservative version Eq. 3 that was used in (Sengupta et al., 2013). There is no necessity for performing any 'symmetrization', which was done before the scheme was used with numerical dissipation given by a combination of fourth and second derivatives (Sengupta et al., 2013). Very satisfactory results have been obtained using the OUCS2 in the form given by Eq. 4, described in the next section.
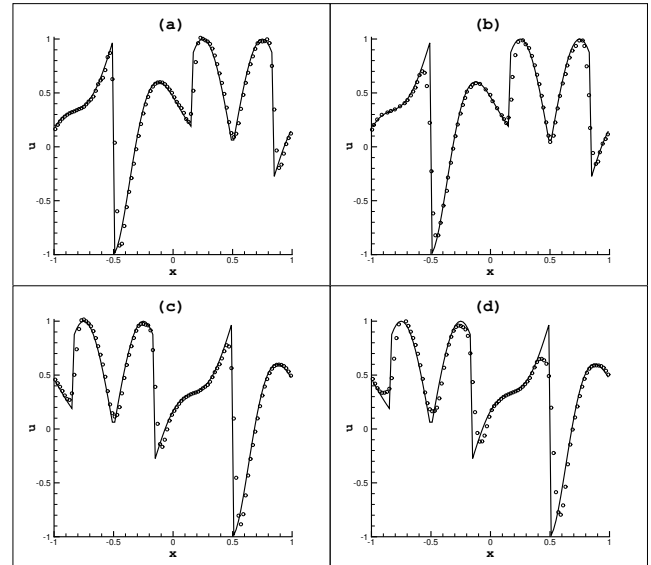

Fig. 2. Solution of the wave equation: (a) OUCS2 with limiter at $t = 2$, (b) Solution given by the a seventh-order WENO scheme coupled with a fifth-order compact scheme at $t = 2$. (c) and (d) are computed by the OUCS2 with limiter at $t = 5$ and 15, respectively. Number of cells $= 100$; CFL $= 0.5$; solid lines: exact solution.

Results and discussion

Having outlined the method of application of the OUCS2 scheme in an AUSM$^+$-based Euler solver, we now focus on a number of standard problems in one and two dimensions to assess the performance of the scheme. In doing so, we must remember that such a scheme of high

spectral accuracy is not needed near shocks. All we expect from the solver is to be able to detect the shock and switch to suitable lower order formulae to avoid oscillatory results. Thus in the test problems we note whether the shock is captured without significant 'wiggles' nearby and whether away from it the smoother variations in the variables are accurately represented by the compact scheme. We have used a four-stage Runge-Kutta scheme given in for time integration in all the problems except the first, where to facilitate comparison of results we have used a different four-stage Runge-Kutta scheme.
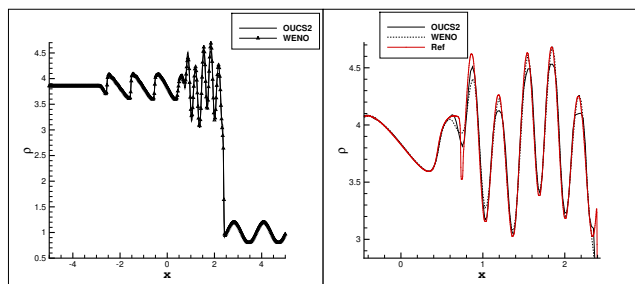
Fig. 3. Interaction of shock and density wave. Left frame: full domain, right frame: zoomed view of the fluctuating density. Results correspond to $t = 1.8$. grid size: 400 cells, CFL $= 0.1$.

Problems in one dimension

We will first solve a linear one dimensional wave propagation problem to demonstrate how the accuracy of the compact scheme can be used to our advantage if a proper limiter is in action. Further, two one dimensional standard test cases are computed solving the Euler equations.

### Wave propagation in one dimension

The governing equation is

$$\frac{\partial u}{\partial t} + \frac{\partial u}{\partial x} = 0. \qquad (6)$$

The initial condition that is specified at $t = 0$ propagates to the right with a speed of $c = 1$. We specify the following discontinuous initial condition:

$$u(x + 0.5) = \begin{cases} -x \sin\left(\frac{3}{2}\pi x^2\right), & -1 \leq x \leq -\frac{1}{3} \\ |\sin(2\pi x)|, & |x| < \frac{1}{3} \\ 2x - 1 - \sin(3\pi x)/6, & \frac{1}{3} \leq x < 1 \end{cases}$$

Periodic boundary conditions are applied at both the ends of the domain. This problem was solved in (Shu and Osher, 1989). In Fig. 2. we compare the result of

the OUCS2 at $t = 2$ with (Pirozzoli, 2002), both computed using 100 cells and the same Runge-Kutta time stepping. At $t = 2$ the initial wave travels a distance of one wavelength, and appears at the same initial position. In (Pirozzoli, 2002) this problem was computed using a seventh-order WENO scheme coupled to a fifth-order compact upwind scheme. It has been shown in (Sengupta et al., 2004) that for such problems it is sufficient to compute the first derivative using a 'strictly one-sided' explicit third-order upwind scheme near discontinuities. The discontinuities were detected by the magnitude of the second derivative. When $|\frac{\partial^2 u}{\partial x^2}| > 50$, the one-sided formula was used, yielding results that were superior to those obtained by the more complex WENO-compact hybrid scheme referred to above. However, the comparison was made using 200 cells, citing greater difficulty in computing with less dissipation associated with more number of cells. We choose to compare with the results in (Pirozzoli, 2002) using the same 100 cells in the domain. Though not shown here, with 200 cells the OUCS2 produces even better results in our mode of application, contrary to the reverse trend noticed in (Sengupta et al., 2004). For wave propagation phenomena in one dimension with discontinuous initial data, it is sufficient to locate the presence of the discontinuities and apply a low-order dissipation. We detect the discontinuities by using Harten's TVD condition in the limiter, and apply a second derivative as artificial dissipation in a conservative manner. Thus we are not using any problem-dependent threshold value, as was done in (Sengupta et al., 2004), and the TVD condition violation proves sufficient to detect the discontinuities. We also do not switch to a fully explicit one-sided form of the first derivative, and the compact scheme is retained near discontinuities - only extra low-order numerical dissipation is added. The Fig. 2. shows that at $t = 2$ (see frames (a) and (b)) the OUCS2 produces better results compared to the compact-WENO scheme.
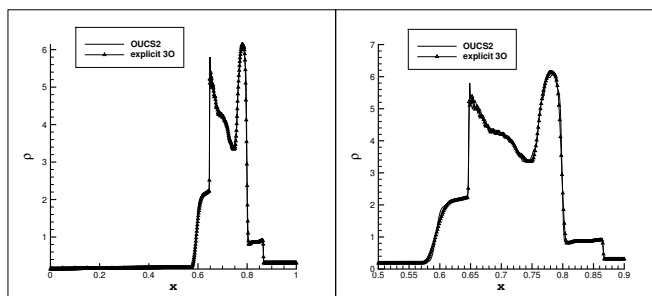
Fig. 4. Interaction of blast waves in one dimension: result at $t = 0.038$. Left frame: full domain, right frame: zoomed view. Grid size: 800 cells, CFL $= 0.1$.

For this kind of problems it is possible to obtain a good match with the exact solution momentarily while the solver actually is on the way to produce oscillatory diverging results at greater time instants. To show that this is not the case with the present form of application of the OUCS2, the frames (c) and (d) are presented, which show the results at $t = 5$ and 15. We notice that the time iterations continue in a stable manner without any new extrema. The effect of inbuilt artificial dissipation of the overall scheme is reflected in reduction of the amplitude with time. The results for this test case proves that in one-dimensional wave propagation problems, use of compact schemes in a conservative form, as in the present case, can be very accurate in combination with a TVD limiter.
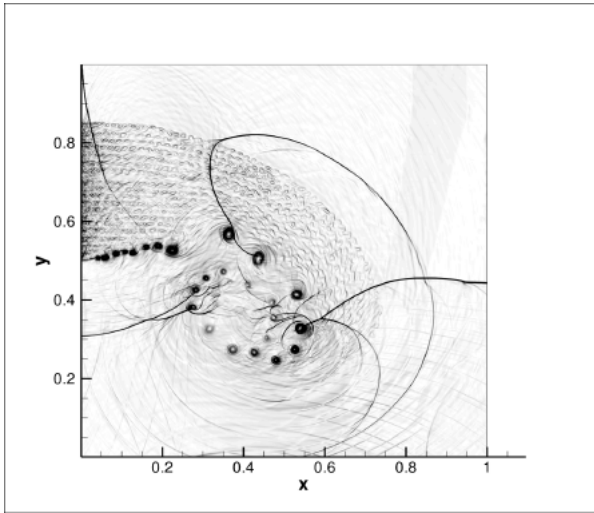
Fig. 5. Shock diffraction at a corner: numerical schlieren at $t = 1$. OUCS2 scheme on 1000×1000 grid. Computed with a constant $\Delta t = 10^{-4}$. 40 contour levels have been plotted from 1 to 40 at an increment of 1.

Shock-density wave interaction

This problem is taken from (Shu and Osher, 1989). A Mach 3 shock interacts with a density wave in a domain $-5 \leq x \leq 5$. The initial condition is

$$(\rho, u, p) = \begin{cases} (3.857143, 2.629369, 10.333333), & x \leq -4 \\ (1 + 0.2\sin(5x), 0, 1), & x > -4 \end{cases}$$

400 cells are taken in the domain. We solve the Euler equations in one dimension and compare results of OUCS2 with the following standard third-order explicit upwind scheme:

$$u_{i+\frac{1}{2}} = \frac{2u_{i+1} + 5u_i - u_{i-1}}{6}. \tag{7}$$

In Fig. 3. the result at $t = 1.8$ is shown. The reference solution is computed on a grid of 4000 cells using a ninth-order explicit scheme. We note that the density fluctuation is better captured by the OUCS2 compared to the third-order explicit scheme. This shows that the limiter is active only in shock-capturing, and the OUCS2 is resolving the smoother fluctuations.
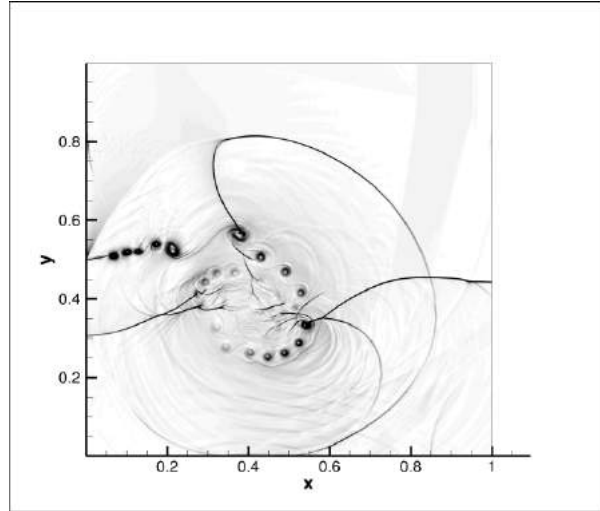
Fig. 6. Shock diffraction at a corner: numerical schlieren at $t = 1$. third-order explicit scheme (Eq. 7) on 1000×1000 grid. Computed with a constant $\Delta t = 10^{-4}$. Same contour levels as in Fig. 5.

Interacting blast waves

For this problem the initial condition is (Shu and Osher, 1989)

$$(\rho, u, p) = \begin{cases} (1, 0, 1000), & 0 \leq x \leq 0.1 \\ (1, 0, 0.01), & 0.1 \leq x < 0.9 \\ (1, 0, 100), & 0.9 \leq x \leq 1 \end{cases}$$

We solve the Euler equations in one dimension using 800 cells and view the result in Fig. 4. Solid wall boundary condition is applied at the ends of the domain. This problem was chosen to highlight the fact that the present compact scheme-limiter combination is able to handle a pressure jump by a factor of 10^5 in the initial conditions. Density variation is generally sharper in the OUCS2 result which is visible in the sharp density rise at $x = 0.6$. If we compare with the results in figure 13 of (Shu and Osher, 1989), we note that the OUCS2 result is comparable to the result of the ENO-RF-S-3 computed on the same grid.

Problems in two dimensions

We now focus on three two dimensional problems which involve both shock waves and vortices. There are problems where high wavenumber excitation is nearly absent. In such cases a high accuracy compact scheme and a lower order explicit scheme produce comparable results. We choose our test cases carefully so that the use of a compact upwind scheme makes a difference when compared with a third-order explicit formula.

Shock diffraction at a corner

This problem is taken from (Artebrant and Schroll, 2006). The domain of interest is a unit square. Initially, the whole of the interior has $u = v = 0$ and $\rho = p = 1$. At the inflow, which is the top half of the left vertical boundary, $p = 3$ and flow angle is $\pi/10$. Solid wall boundary conditions are set at the lower half of the left boundary and the bottom wall. Artificial absorbing boundary condition is set at the top and right walls. This is similar to the Schardin's problem (Halder et al., 2013), but the present domain is small and set-up of the problem much easier.
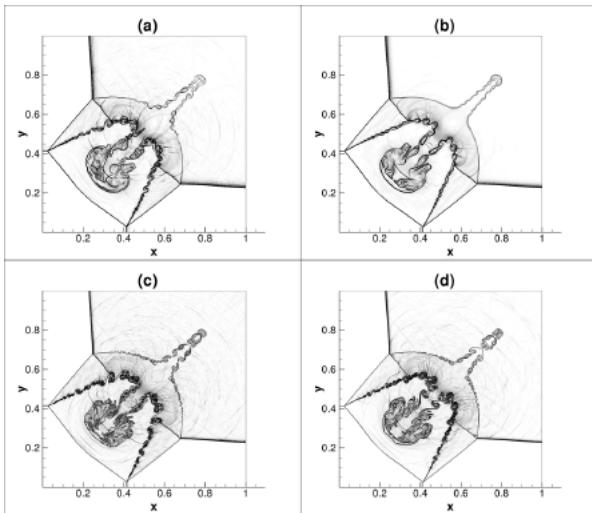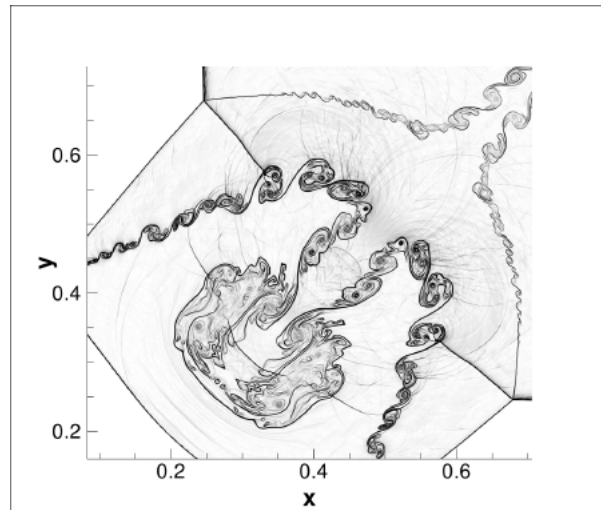

Fig. 7. The four-shocks problem: numerical schlieren at $t = 0.8$. (a) OUCS2 on 1000×1000 grid, (b) third-order scheme on 1000×1000 grid, (c) OUCS2 on 2400×2400 grid, (d) third-order scheme on 2400×2400 grid. CFL = 0.5 for all. 40 contour levels with an increment of 1.

Note that the initial condition is not fully correct in (Artebrant and Schroll, 2006). The shock wave that is part of the initial condition diffracts at the corner ($x = 0$, $y = 0.5$ - the point separating the inflow and the wall boundary condition at the left vertical boundary).

The diffracted shock is later reflected back into the domain at the bottom wall. Meanwhile, a vortex grows

behind it near the inflow. When the reflected shock moves upward, it interacts with this primary vortex. Small-scale vortices are also noticed behind the primary vortex. These are generated due to the Kelvin-Helmholtz instability. In Fig. 5., we notice these small-scale vortices moving into the primary core. The reflected shock interacts with the primary vortex. It cannot pass through the vortex with its shape intact, and breaks into accelerated and decelerated components - visible in Fig. 5.

In Fig. 6., the solution produced by the third-order scheme (Eq. 7) is shown. Comparing, we note that the OUCS2 result has more small-scale trailing vortices. This is indicative of the high wavenumber accuracy of the OUCS2. Similar vortices are also generated behind a shock-tube generated vortex ring (Murugan et al., 2012). Using a second-order accurate scheme, these could not be detected as early as they could be seen in experiments. OUCS2 or a similar scheme is likely to detect these small-scale vortices better. The background disturbance in the OUCS2 result occurs for other high resolution schemes also. This has been tested by us using another high resolution scheme. This is likely to be the result of artificial inflow boundary condition applied here. This disturbance remains undetected by third order accurate schemes.

Fig. 8. The four-shocks problem: numerical schlieren at $t = 0.8$. OUCS2 on 2400×2400 grid. High wavenumber accuracy of the OUCS2 generates the smaller-scale structures that would not be visible by lower accuracy schemes. 50 contour levels are drawn between 1 to 99 at an increment of 2.

The four-shocks problem

In this problem, the initial condition contains four shocks - dividing the unit square domain into four quadrants. The variables are set as

$$(\rho, u, v, p) = \begin{cases} (1.5, 0, 0, 1.5) , & Q1 \\ (0.53225806, 1.20604538, 0, 0.3) , & Q2 \\ (0.13799283, 1.20604538, 1.20604538, \\ \quad 2.90322581 \times 10^{-2}), & Q3 \\ (0.53225806, 0, 1.20604538, 0.30) , & Q4 \end{cases}$$

where $Q1 : [0.75, 1] \times [0.75, 1]$; $Q2 : [0, 0.75] \times [0.75, 1]$; $Q3 : [0, 0.75] \times [0, 0.75]$ and $Q4 : [0.75, 1] \times [0, 0.75]$.

The full description is provided in (Schulz-Rinne et al., 1993). We keep the point of contact of the four shocks at $(x = 0.75, y = 0.75)$, instead of at the centre of the domain. This was also done in (Serna, 2006) for better visualization of the results. We did not type in the values given above, rather (Schulz-Rinne et al., 1993) was consulted for analytical expressions whenever available. With time, four slip lines develop. In Fig. 7. the results of the OUCS2 and the third-order explicit scheme, given by Eq. 7, are plotted for two different grid sizes - 1000×1000 and 2400×2400. Both the OUCS2 and the third-order scheme produce the key structures similar to the ones in published literature (Schulz-Rinne et al., 1993; Serna, 2006; Čada and Torrilhon, 2009). The last reference solved this problem on a 1000×1000 grid using a second-order accurate TVD-MUSCL scheme with various limiters. For a certain limiter (designated LimO3), the roll-up of the slip lines was most prominent.
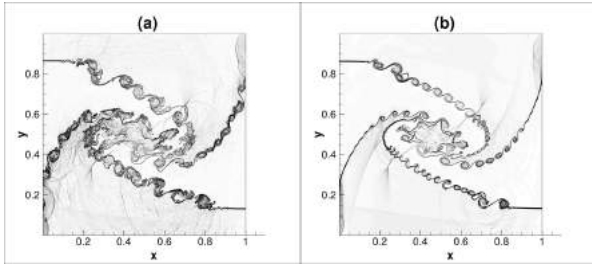
Fig. 9. The four-contacts problem: numerical schlieren at $t = 0.8$. (a) OUCS2 and (b) third-order scheme on 2400×2400 grid. CFL $= 0.5$. 50 contour levels are drawn between 1 to 99 at an increment of 2.

In our case, this roll-up is much stronger for the OUCS2 scheme on the same grid. The third-order scheme also produces roll-up structures, but to a less extent. On the 2400×2400 grid, the OUCS2 creates small scale details which are resolved only due to its high spectral accuracy for a larger wavenumber range. This is shown more clearly in Fig. 8., which shows a zoomed view of the central region. The finer details visible in this figure confirm the suitability of the OUCS2 for shock-vortex interaction cases where small-scale structures are generated.

The four-contacts problem

The initial condition for the four-contacts problem is given by (Schulz-Rinne et al., 1993)

$$(\rho, u, v, p) = \begin{cases} (1.0, 0.75, -0.50, 1.0) , & Q1 \\ (2.0, 0.75, 0.50, 1.0) , & Q2 \\ (1.0, -0.75, 0.50, 1.0 \times 10^{-2}) , & Q3 \\ (3.0, -0.75, -0.50, 1.0) , & Q4 \end{cases}$$

where $Q1 : [0.5, 1] \times [0.5, 1]$; $Q2 : [0, 0.5] \times [0.5, 1]$; $Q3 : [0, 0.5] \times [0, 0.5]$ and $Q4 : [0.5, 1] \times [0, 0.5]$.
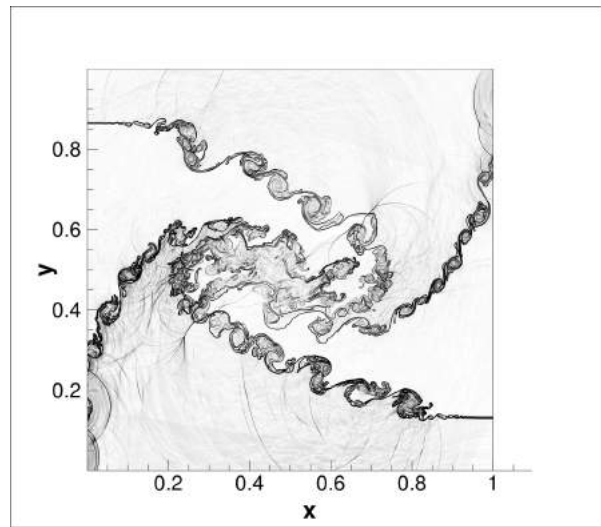
Fig. 10. The four-contacts problem: numerical schlieren at $t = 0.8$. (a) OUCS2 on 2400×2400 grid: zoomed view to show the small-scale structures. Same contour levels as in Fig. 9.

The solution is a clockwise turning vortex with four slip lines spiralling around the centre (Schulz-Rinne et al., 1993). For this problem, the conditions listed above can be typed in, and no analytical expression is involved for accurate representation. Here also the slip lines generate roll-up vortices. Results are plotted in the form of numerical schlieren at $t = 0.8$ in Fig. 9. From our simulation results and the ones in (Čada and Torrilhon, 2009), we note that the slip lines which extend to the first and the third quadrants are the ones which develop the smaller scale vortices. In fact, these slip lines do not show any such vortices prominently in (Čada and Torrilhon, 2009) for the second-order TVD-MUSCL scheme with any of the limiters used on a 1000×1000 grid. Only the slip lines extending to the second and the fourth quadrants develop a couple of roll-up vortices. In our case a similar trend is observed. In Fig. 9., the slip lines in the second and the fourth quadrants display these roll-up structures all along their length for both OUCS2

and the third-order scheme. In the other two quadrants, only OUCS2 is able to excite these structures along the whole length of the slip lines. The third-order scheme does not show these near the outer ends. Fig. 10. is a zoomed view of the central region for OUCS2. The interior of the rolled-up structures now show even smaller-scale features. The third-order scheme is unable to produce them, and this is where a fifth-order upwind compact scheme like the OUCS2 can be most effectively used.

Concluding remarks

We have presented a method of application of the OUCS2 upwind compact scheme for compressible flow problems with shocks. The OUCS2 is a fifth-order upwind compact scheme with artificial dissipation provided by a sixth-derivative. Our approach enables applying the OUCS2 scheme to its full strength, and not by application of lower-order (fourth) dissipation explicitly, as has been done in recent literature. We apply the OUCS2 in a conservative manner, instead of losing discrete conservation due to its use in the derivative form coupled with switches to identify shocks. No symmetrization is performed, and the OUCS2 is integrated into an AUSM$^+$-based Euler solver equipped with TVD limiting. A number of test cases in one and two dimensions indicate that accurate results can be obtained by the present approach. For one-dimensional linear wave propagation with discontinuous initial condition, the OUCS2 combines well with a TVD limiting strategy to capture the solution more accurately in comparison to a seventh-order WENO scheme hybridized with a fifth-order compact scheme. Two other standard one-dimensional problems of gas dynamics show the accuracy of the OUCS2 in smooth regions and its ability to combine with the TVD limiting procedure to predict evolution of sharp jumps in the initial condition. The two-dimensional problems have small-scale vortices and shocks/slip lines developing into an unsteady flow-field. The OUCS2 has been shown to be effective in capturing these small-scale structures much better than a standard third-order explicit scheme. Such structures are part of many shock-vortex and shock-turbulence interaction problems, and this is where we plan to apply the OUCS2 and other high spectral accuracy schemes in future.

References

Artebrant, R. and Schroll, H. J. (2006). Limiter-free third-order logarithmic reconstruction. *SIAM J. Sci. Comput.* 28(1):359–381.

De, S. and Murugan, T. (2011). Numerical simulation of shock tube generated vortex: effect of numerics. *Int. J. Comput. Fluid Dyn.* 25(6):345–354.

Dora, C. L., Murugan, T., De, S. and Das, D. (2014). Role of slipstream instability in formation of counter-rotating vortex rings ahead of a compressible vortex ring. *J. Fluid Mech.* 753:29–48.

Hahn, M. and Drikakis, D. (2009). Assessment of large-eddy simulation of internal separated flow. *J. Fluids Eng.* 131(071201).

Halder, P., De, S., Sinhamahapatra, K. P. and Singh, N. (2013). Numerical simulation of shock-vortex interaction in schardin's problem. *Shock Waves.* 23:495–504.

Jiang, G. S. and Shu, C. W. (1996). Efficient implementation of weighted eno schemes. *J. Comput. Phys.* 126:202–228.

Kawai, S., Shankar, S. K. and Lele, S. K. (2010). Assessment of localized artificial-difusivity scheme for compressible turbulent flows. *J. Comput. Phys.* 229:1739–1762.

Kundu, A. and De, S. (2014). High resolution euler simulation of a cylindrical blast wave in an enclosure. *J. Vis.* 18:733–738.

Liou, M. S. (1996). A sequel to the ausm: Ausm$^+$. *J. Comput. Phys.* 129:364–382.

Meinke, M., Schroder, W., Krause, E. and Rister, T. (2002). A comparison of second- and sixth-order methods for large-eddy simulations. *Comput. Fluids.* 31:695–718.

Murugan, T., De, S., Dora, C. L. and Das, D. (2012). Numerical simulation and piv study of compressible vortex ring evolution. *Shock Waves.* 22:69–83.

Pirozzoli, S. (2002). Conservative-hybrid compact-weno schemes for shock-turbulence interaction. *J. Comput. Phys.* 178:81–117.

Ravichandran, K. S. (1994). Flux limited non-oscillatory cud-3 schemes for 1-d euler equations. *Int. J. Comput. Fluid. Dyn.* 3:141–152.

Ravichandran, K. S. (1997). Explicit third order compact upwind difference schemes for compressible flow calculations. *Int. J. Comput. Fluid. Dyn.* 8:311–316.

Rizzetta, D. P. and Morgan, P. E. (2008). A high-order compact finite-difference scheme for large eddy simulation of active flow control. *Prog. Aerosp. Sci.* 44:397–426.

Schulz-Rinne, C. W., Collins, J. P. and Glaz, H. M. (1993). Numerical solution of the riemann problem for two-dimensional gas dynamics. *SIAM J. Sci. Comput.* 14(6):1394–1414.

Sengupta, T. K., Bhole, A. and Sreejith, N. A. (2013). Direct numerical simulation of 2d transonic flows around airfoils. *Comput. Fluids.* 88:19–37.

Sengupta, T. K., Ganeriwal, G. and De, S. (2003). Analysis of central and upwind compact schemes. *J. Comput. Phys.* 192:677–694.

Sengupta, T. K., Ganerwal, G. and Dipankar, A. (2004). High accuracy compact schemes and gibbs' phenomenon. *J. Sci. Comput.* 21(3):253–268.

Serna, S. (2006). A class of extended limiters applied to piecewise hyperbolic methods. *SIAM J. Sci. Comput.* 28(1):123–140.

Shu, C. W. and Osher, S. (1989). Efficient implementation of essentially non-oscillatory shock-capturing schemes, ii. *J. Comput. Phys.* 83:32–78.

Tolstykh, A. I. (1973). On a method for the numerical solution of navier-stokes equations of a compressible gas over a wide range of reynolds numbers. *Dokl. Akad. Nauk.* 210(1):48–51.

Tolstykh, A. I. (1994a). High-accuracy non-centered compact difference schemes for fluid dynamics applications. *World Scientific.*, Singapore.

Tolstykh, A. I. and Lipavskii, M. V. (1998). On performance of methods with third- and fifth-order compact upwind differencing. *J. Comput. Phys.* 140:205–232.

Tolstykh, M. A. (1994b). Application of fifth-order compact upwind differencing to moisture transport in the atmosphere. *J. Comput. Phys.* 112:394–403.